EXTERNAL CONVECTIVE MASS TRANSFER OF A PLATE IN A NON-NEWTONIAN LIQUID

A. V. Luikov, Z. P. Shul'man, and B. I. Puris

Inzhenerno-Fizicheskii Zhurnal, Vol. 14, No. 6, pp. 961–974, 1968

UDC 532.517.2:532.135

The local mass transfer of a flat plate in a longitudinal non-Newtonian fluid flow has been analytically and experimentally investigated. The agreement between experiment and calculation is completely satisfactory. The effect of the rheological characteristics of the solution on the location of the laminar-turbulent boundary layer transition has been established.

In recent years, there has been a considerable increase of interest in problems of convective transport in non-Newtonian fluids. Against the fairly extensive background of publications on rheodynamics and heat transfer in fluid systems of a general type, theoretical and experimental studies of mass transfer are conspicuous by their absence. At the same time, problems of this class are important in theory as well as in practice, since diffusion in non-Newtonian disperse systems and polymer solutions has its own particular characteristics that distinguish it from the heat transfer process. In particular, the coefficient of diffusion of a polymer in a low-molecular-weight medium is not only several orders lower than the thermal conductivity of the same solution, but also exhibits an exceptionally strong and nonlinear concentration dependence, whereas the thermal conductivity varies only very slightly. As yet there have been no studies of the effect of the rheological characteristics of shear flow on the convection of an additive under the conditions of the external and internal problems.

This article reports the results of an analytic and experimental investigation of the mass transfer in the boundary layer on a plate in a longitudinal flow of so-called "power-fluid-law" non-Newtonian fluid.

Analytic investigation. The starting system for the plane problem of a laminar boundary layer is written in the form

$$\rho u \frac{\partial u}{\partial x} + \rho v \frac{\partial u}{\partial y} = kn \left| \frac{\partial u}{\partial y} \right|^{n-1} \frac{\partial^2 u}{\partial y^2}, \tag{1}$$

$$\frac{\partial u}{\partial x} + \frac{\partial v}{\partial y} = 0, \tag{2}$$

$$\tau = k \left| \frac{du}{dy} \right|^{n-1} \frac{du}{dy}, \tag{3}$$

$$\rho u \frac{\partial c}{\partial x} + \rho v \frac{\partial c}{\partial y} = \frac{\partial}{\partial y} \left[\rho D \frac{\partial c}{\partial y} \right]. \tag{4}$$

The velocity distribution given by (1)–(3) is assumed known. It is given in [1] in the form of tables and graphs. We solve Eq. (4) on the assumption of diffusion kinetics, i.e., for the boundary conditions of limiting diffusion flow. We also assume that diffusion does not take place over the entire flow surface but begins at a certain distance h_0 reckoned from the leading edge of the plate. Consequently, the portion of the plate $0 \leq x \leq h_0$ is characterized by the condition $j = 0$ (passive part of plate).

For all $x > h_0$ (active part) the condition $c = 0$ holds. From physical considerations it is clear that the limiting flow regime on this part of the plate is not established immediately beyond the passive section. On a certain part of the active surface there will be a transition to the limiting flow, and here the diffusion mass transfer will be higher than the corresponding limiting value reached at $x \gg h_0$. In this region—let us call it the stabilization region—longitudinal mass transfer makes a greater contribution to the total diffusion flux than in the region of the steady-state limiting regime. Passing from the physical coordinates x and y to the variables x and Ψ, we reduce Eq. (4) to the form

$$\left(\frac{\partial c}{\partial x} \right)_\Psi = \frac{\partial}{\partial \Psi} \left[Du \frac{\partial c}{\partial \Psi} \right]. \tag{5}$$

The new abscissa x is now reckoned along the streamline $\Psi = \text{const}$ (in what follows the subscript Ψ indicating this fact will be omitted). The variable Ψ is reckoned from the wall ($\Psi = 0$). Equation (5) must be solved for the following boundary conditions:

$$\frac{\partial c}{\partial \Psi} = 0 \quad \text{at} \quad \Psi = 0 \quad (x < h_0), \tag{6}$$

$$c = 0 \quad \text{at} \quad \Psi = 0 \quad (x > h_0), \tag{7}$$

$$c = c_0 \quad \text{at} \quad \Psi = 0 \quad (x = 0), \tag{8}$$

$$c = c_0 \quad \text{as} \quad \Psi \to \infty. \tag{9}$$

To relate the quantities u, x, and Ψ, we used the known self-similar solutions of the dynamic problem for a plate [1],

$$\eta = y x^{-\frac{1}{1+n}} \left[\frac{U_\infty^{2-n} \rho}{n(n+1)k} \right]^{\frac{1}{1+n}} = y x^{-\frac{1}{1+n}} M^{\frac{1}{1+n}}, \tag{10}$$

$$u = U_\infty \frac{dF(\eta)}{d\eta}, \quad \Psi = x^{\frac{1}{1+n}} U_\infty M^{-\frac{1}{1+n}} F(\eta),$$

$$M = \left[\frac{U_\infty^{2-n} \rho}{n(n+1)k} \right]. \tag{11}$$

The required function $\eta(\Psi)$ is established from the expressions

$$u = \frac{\partial \Psi}{\partial y} \text{ and } v = -\frac{\partial \Psi}{\partial x}, \tag{12}$$

satisfying the continuity equation (2).

All liquids (particularly highly viscous ones) are characterized by the condition $\mathrm{Pr_m} \gg 1$. Then the diffusion boundary layer is much thinner than the dynamic boundary layer, within which it occupies a narrow region near the wall. Hence, in finding the concentration field from Eq. (5) it is necessary to consider not the total velocity profile but only the part "immersed" in the diffusion boundary layer. It is customary to employ for this purpose the one-parameter linear family

$$\frac{u}{U_\infty} = \beta_1(x, n)\, y = \left[\frac{\partial (u/U_\infty)}{\partial \eta}\right]_{\eta=0} \eta, \tag{13}$$

where

$$\beta_1 = \left(\frac{\partial u/U_\infty}{\partial \eta}\right)_{\eta=0} x^{-\frac{1}{n+1}} M^{\frac{1}{n+1}}.$$

Combining (10)–(13), we arrive at the relation

$$\eta = 2^{1/2} x^{-\frac{1}{2(n+1)}} \beta_1^{-1/2} M^{\frac{1}{2(1+n)}} U_\infty^{-1/2} \Psi^{1/2}. \tag{14}$$

Equation (5) now simplifies to

$$x^{\frac{1}{2(n+1)}} \frac{\partial c}{\partial x} = B \frac{\partial}{\partial \Psi}\left(\sqrt{\Psi} \frac{\partial c}{\partial \Psi}\right). \tag{15}$$

Here,

$$B = 2^{1/2} D \beta_1^{1/2} U_\infty^{1/2} M^{\frac{1}{2(n+1)}}. \tag{16}$$

We introduce the new variables

$$\xi = \frac{n+1}{2(2n+1)} B x^{\frac{2n+1}{2(n+1)}}; \quad \varphi = \sqrt{\Psi}. \tag{17}$$

As a result, we arrive at the new notation,

$$\frac{\partial c}{\partial \xi} = \frac{1}{\varphi} \frac{\partial^2 c}{\partial \varphi^2}, \tag{18}$$

$$c \to c_0 \quad \text{as} \quad \varphi \to \infty, \tag{19}$$

$$\frac{\partial c}{\partial \varphi} = 0 \quad \text{at} \quad \xi < \frac{n+1}{2(2n+1)} B h_0^{\frac{2n+1}{2(n+1)}} \text{ and } \varphi = 0, \tag{20}$$

$$c = 0 \quad \text{at} \quad \xi > \frac{1}{2} \frac{n+1}{2n+1} B h_0^{\frac{2n+1}{2(n+1)}} \text{ and } \varphi = 0. \tag{21}$$

Following [2], we first find the solution of the limiting boundary value problem in the variables ξ and φ for a semi-infinite plate without an initial passive section ($h_0 = 0$). Then the boundary conditions simplify to

$$c \to c_0 \quad \text{as} \quad \varphi \to \infty, \tag{22}$$

$$c = 0 \quad \text{at} \quad \varphi = 0, \tag{23}$$

$$c = c_0 \quad \text{at} \quad \xi = 0; \quad \varphi = 0. \tag{24}$$

The change of variables

$$\omega = \varphi (9\xi)^{-1/3} \tag{25}$$

leads to the equation

$$\frac{d^2 c}{d\omega^2} + 3\omega^2 \frac{dc}{d\omega} = 0. \tag{26}$$

The solution of (26) is

$$c_{\lim} = \frac{c_0 \int_0^\omega e^{-\lambda^3} d\lambda}{\int_0^\infty e^{-\lambda^3} d\lambda} = c_0 \left[\frac{1}{3}\Gamma\left(\frac{1}{3}\right)\right]^{-1} \int_0^\omega e^{-\lambda^3} d\lambda. \tag{27}$$

Equation (18) is invariant under the group of displacement transformations $\xi + \xi_0$ ($\xi_0 = \text{const}$). We select

$$\xi_0 = -\frac{B}{2} \frac{n+1}{2n+1} h_0^{\frac{2n+1}{2(n+1)}}.$$

The function

$$c = c_0 \left[\frac{1}{3}\Gamma\left(\frac{1}{3}\right)\right]^{-1} \int_0^\zeta \exp(-\lambda^3) d\lambda,$$

$$\zeta = \frac{\varphi}{\sqrt[3]{9}\left(\xi - \frac{B}{2} \frac{n+1}{2n+1} h_0^{\frac{2n+1}{2(n+1)}}\right)^{1/3}} \tag{28}$$

satisfies Eq. (18) and conditions (19)–(21).

In the physical variables the solution has the form

$$c(x, y) = \begin{cases} c_0 & \text{at } x < h_0, \\ c_0 \left[\frac{1}{3}\Gamma\left(\frac{1}{3}\right)\right]^{-1} \int_0^p \exp(-\lambda^3) d\lambda & \end{cases}$$

$$\text{at } x > h_0; \quad p = \frac{1}{\sqrt{2}} \left[\frac{2n+1}{9(n+1)}\right]^{\frac{1}{3}} \times$$

$$\times D^{-\frac{1}{3}} \beta_1^{\frac{1}{6}} U_\infty^{\frac{1}{3}} M^{\frac{1}{3(n+1)}} y x^{-\frac{n+2}{3(n+1)}} \times$$

$$\times \left[1 - \left(\frac{h_0}{x}\right)^{\frac{2n+1}{2(n+1)}}\right]^{-1/3}. \tag{29}$$

The diffusion flux density on the active sections is given by the relation

$$j = D\left(\frac{\partial c}{\partial y}\right)_{y=0} =$$

$$= c_0 \left[\frac{1}{3}\Gamma\left(\frac{1}{3}\right)\right]^{-1} \left[\frac{2n+1}{36(n+1)}\right]^{\frac{1}{3}} \times$$

$$\times B^{2/3} x^{-\frac{n+2}{3(n+1)}} \left[1 - \left(\frac{h_0}{x}\right)^{\frac{2n+1}{2(n+1)}}\right]^{-1/3}. \tag{30}$$

At n = 1 (Newtonian fluid) relations (29) and (30) automatically go over into the Maiman solution [2].

The ratio of the true and limiting ($h_0 = 0$) diffusion fluxes is expressed by the simple equation

$$\frac{j}{j_{\lim}} = \left[1 - \left(\frac{h_0}{x}\right)^{\frac{2n+1}{2(n+1)}}\right]^{-1/3}. \quad (31)$$

Thus, the amount by which the true flux j exceeds $j_{\lim}$ and the extent of the stabilization region depend not only on the ratio h_0/x but also on the index n of non-Newtonian behavior.

For pseudoplastic fluids, the development of the $j_{\lim}$ regime requires a greater length x than for Newtonian fluids. Dilatant systems exhibit the opposite tendency. The exponent of the ratio h_0/x varies from 1/2 (pseudoplastic limit, $n = 0$) to 1 (extreme dilatancy, $n \to \infty$). For a fixed value of h_0 the abscissa at which j and $j_{\lim}$ differ, for example, by 5% is $x_5\% \cong 10h_0$ for the maximally pseudoplastic fluid, $x_5\% \cong 5h_0$ for a Newtonian fluid, and $x_5\% \cong 3h_0$ for the maximally dilatant system.

The solution obtained has two important consequences. First, the effect of the initial passive section is manifested the more strongly, the lower the value of n. This is due to the increased contribution of the tangential component to the total transverse mass flux. In the case of large h_0/L, the transferable transverse mass flux density on the entire active part of the plate differs considerably from $j_{\lim}$, despite the fact that, as before, the process proceeds in the diffusion region and the condition $c|_{y=0} = 0$ is satisfied.

Second, the device of an initial passive section provides a means of controlling convective mass transfer in a non-Newtonian fluid. New possibilities are created for the optimum control of mass transfer processes in the production and processing of polymers and plastics in the fluid state.

We transform the solution obtained to the dimensionless form

$$\mathrm{Nu}_{mx} = \left\{\frac{\beta_1}{0.89^3 \cdot 18}\frac{2n+1}{n+1}[n(n+1)]^{-\frac{1}{1+n}}\right\}^{1/3} \times$$
$$\times \mathrm{Re}_x^{\frac{1}{1+n}} \mathrm{Pr}_{mx}^{\frac{1}{3}} \left[1 - \left(\frac{h_0}{x}\right)^{\frac{2n+1}{2(n+1)}}\right]^{-1/3} \quad (32)$$

and determine the values of the j fluxes averaged on the section $x-h_0$:

$$\bar{j}_x = \frac{1}{x - h_0}\int_{h_0}^{x} j\,dx =$$
$$= \frac{3(n+1)}{2n+1} A h_0^{-\frac{n+2}{3(n+1)}} \frac{\left[\left(\frac{x}{h_0}\right)^{\frac{2n+1}{2(n+1)}} - 1\right]^{2/3}}{\frac{x}{h_0} - 1}. \quad (33)$$

Here

$$A = c_0 \sqrt{\frac{\beta_1 D^2 U_\infty^{\frac{2-n}{1-n}}(2n+1)}{0.89^3 \cdot 18(n+1)\left[\frac{nk}{\rho}(n+1)\right]^{\frac{1}{1+n}}}}. \quad (34)$$

The formulas obtained contain the form parameter of the velocity field, β_1—the only characteristic not amenable to direct measurement. However, its value can be borrowed from the solutions of the self-similar problem of the boundary layer on a semi-infinite plate or from empirical formulas for the friction stress:

$$\beta_1 = \left(\frac{\partial u/U_\infty}{\partial \eta}\right)_{\eta=0} = \frac{d^2F}{d\eta^2}\bigg|_{\eta=0} =$$
$$= \left(\frac{c_f}{2}\right)^{\frac{1}{n}} [n(n+1)]^{\frac{1}{1+n}} \mathrm{Re}_x^{-\frac{1}{n(n+1)}}.$$

Detailed tables of F"(0) for various $0 \leq n \leq 2$ (in steps of 0.1) are given in [1].

Experimental. The experimental method was based on visualization of the convective mass transfer in a liquid electrolyte to which electrochemiluminescent substances (ECL) had been added. If two inert electrodes are introduced into such a solution, a blue luminescence appears at the surface of the anode. At a fixed electrode potential, its local intensity is strictly proportional to the local diffusion flux j(x). References [3, 4] include a detailed description of the ECL method and its application to the investigation of mass transfer and the hydrodynamics of flow around blunt bodies (separation, cavities, wakes, etc.) in Newtonian fluids. The advantages of the method include the fact that it is free of inertia and the disturbances usually introduced by the presence of transducers in the flow. Besides water (solvent), the ECL solution used in the experiments contained hydrogen peroxide (oxidizer, active electrolyte), luminol (the chemiluminescent agent), the sodium salt of carboxymethyl cellulose (non-Newtonian pseudoplastic component), potassium chloride (main electrolyte, so-called background), and sodium hydroxide (pH regulator).

The experiments were conducted at the preselected optimum value of the limiting current ensuring that, on the active surface of the anode, the condition $c_{H_2O_2} = 0$, assumed in the theoretical calculations, was satisfied.

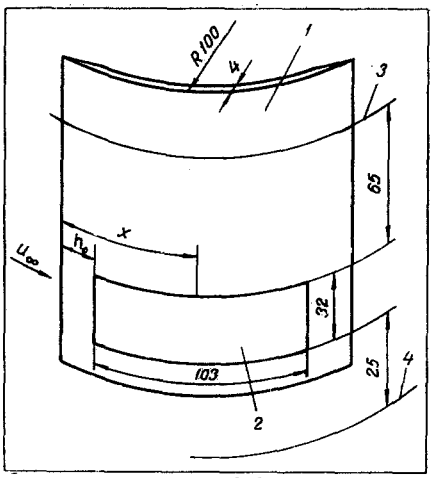

Fig. 1. Diagram of the experimental plate: 1) base; 2) active part of plate (anode); 3) free surface of solution; 4) level of bottom of apparatus.

The experimental apparatus and its organization are described in [5]. The experimental body (anode) was a rectangular platinum plate (active part) bonded with epoxy adhesive to a thin plexiglas sheet bent in a circular arc 100 mm in radius so that part of a cylindrical surface was obtained (Fig. 1). In the presence of an attached uniform coaxially rotating flow, this model is hydrodynamically equivalent to a flat plate in a longitudinal translational fluid flow. The rates of rotation of the vessel were selected so as to eliminate the effect of the centrifugal forces tending to distort the free surface and prevent the development of waves and instabilities. The platinum plate could be secured at various distances from the sharpened leading edge. Thus, we were able to fix the variable ratio of the lengths of the passive (h_0) and active parts of the plate (Fig. 1). Measurements were made at h_0 = 7, 23, and 51 mm (i.e., $h_0/(L + h_0) = 0$; 0.64; 0.18; 0.33); the Na CMC concentration in the experiments was (%): 0; 0.1; 0.25; 0.5; 0.75; 1; 1.5; 2. The velocity of the solution relative to the fixed plate varied from 10 to 50 cm/sec. As indicated by estimates [6] and verified by visual observation, the distances separating the model from the free surface and the lateral walls successfully excluded hydrodynamic interference and various side effects.

A special series of experiments was devoted to the determination of the calibration coefficient k of the apparatus which establishes the direct proportionality of the photocurrent and the diffusion flow to the wall. The absolute value of k depends on the optical properties of the solution, the geometry of the apparatus, the distance between the sensitive element of the photomultiplier and the platinum plate, and on the characteristics of the photomultiplier. The optical properties of the solutions (absorption, refraction) varied somewhat with increase in Na CMC concentration owing to the increased turbidity of the solution. The attenuation of the light signal was measured with a standard photoelectric colorimeter. As a result, we obtained the following relation between the transmittance $T = I_1/I_0$ and the concentration c of the Na CMC component:

$$T = (1.0 + 24c)^{-1} \qquad (35)$$

(I_0 and I_1 are the intensities of the incident and transmitted light fluxes, respectively).

The dependence of the refractive index on the polymer concentration in the electrolyte, obtained in our measurements with an IRF-22 refractometer, was linear and is approximated by the equation

$$n = 1.3413 + 0.124C. \qquad (36)$$

To detect the chemiluminescence, we used an FEU-35 photomultiplier. The test plate (anode) was arranged in one of its focal planes. As a check revealed, the selected instrument has a linear characteristic over the entire measurement range; i.e., the output photocurrent is strictly proportional to the intensity of the anode luminescence. The calibration coefficient k of the apparatus was determined from the previously obtained formula (30). For all values of x and U_∞ we obtained the same value $k = 2.55 \times 10^{-7}$ ($g/\mu A \cdot sec$).

Before beginning the actual experiments we made certain viscometric measurements and also experimentally determined the dependence of the diffusion coefficient of the active electrolyte on the concentration of the non-Newtonian component Na CMC. Rheometric data on the shear viscosity, obtained with a capillary instrument and analyzed in accordance with the Mooney-Rabinovich equation, were found to be closely correlated with the rheological power equation over the entire range of shear rates $(10^2–5 \cdot 10^3)$ sec^{-1}. Values of the parameters n and k for various Na CMC concentrations are presented in [5], which also contains the viscoelastic properties of similar solutions taken from [7].

Our D(c) curve obtained on the basis of refractometer measurements by the method described in detail in [8] is presented in Fig. 2. The sharply nonlinear character and nonmonotonicity of the concentration dependence of the diffusion coefficient are a distinctive feature of solutions containing macromolecules. Consequently, the correct mathematical solution of the problem of convective mass transfer should begin with a nonlinear formulation that takes into account the variability of the diffusion coefficient and the presence of a maximum on the D(c) curve.

Figure 3 gives the results of measurements at various concentrations of the non-Newtonian component for a plate without an initial passive section ($h_0 = 0$). The systematic distribution of the experimental data is noteworthy; deviations from linearity are observed only at large values of U_∞/x (near the leading edge) and at $\lg U_\infty/x < 1$ (region of laminar-turbulent transition). The graphs very accurately reflect the break in the linear distribution of the experimental points, which may be treated as a result of the disturbance of the laminar structure of the boundary layer and transition to the turbulent mass transfer regime. This is confirmed by the agreement between the values of $Re_{cr} = U_\infty x_{cr}/\nu$ obtained in our experiments and the published data for Newtonian fluids. An exact comparison of the values of Re_{cr} is not possible owing to inevitable differences in the degree of freestream turbulence.

As far as non-Newtonian fluids are concerned, nothing based on direct observations has yet been published regarding the transition point (region) on a plate

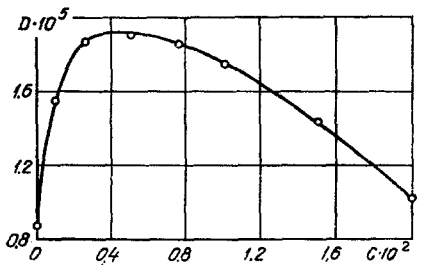

Fig. 2. Diffusion coefficient (cm^2/sec) as a function of the Na CMC concentration (g/cm^3).

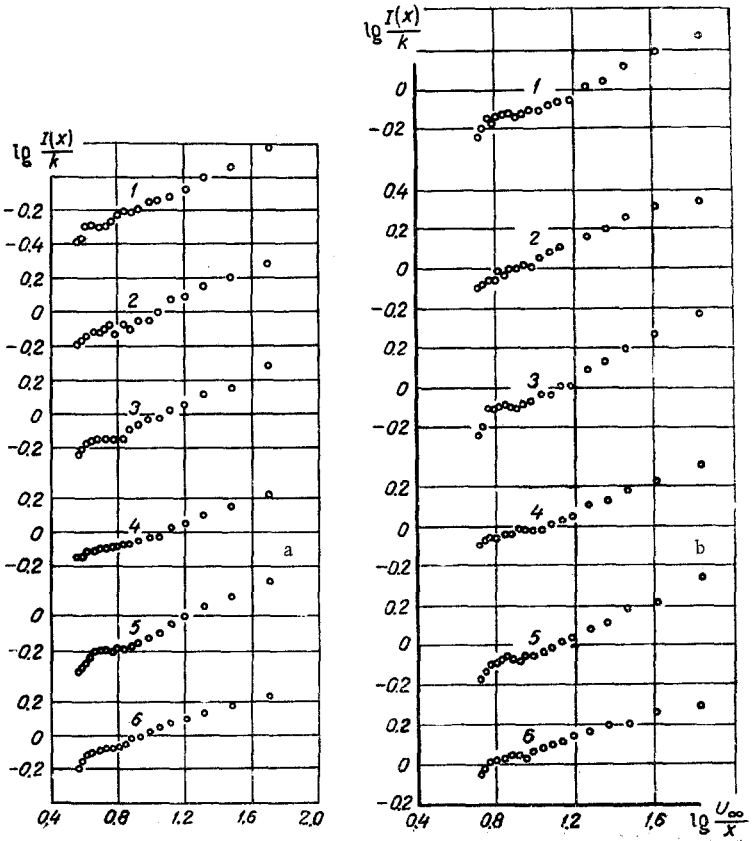

Fig. 3. Mass transfer in the laminar and turbulent regions of the boundary layer as a function of Na CMC concentration: (a) 1) C_{CMC} = 0%; Re_{cr} = 25635; 2) 0.25% and 9908; 3) 0.5% and 4919; 4) 0.75% and 2030; 5) 1% and 1000; 6) 1.5% and 325; (b) 1) C_{CMC} = 0%, Re_{cr} = 25544; 2) 0.25% and 12424; 3) 0.5% and 6879; 4) 0.75% and 3422; 5) 1% and 1378; 6) 1.5% and 437.

in a longitudinal flow. Therefore, the data presented for the first time in Fig. 3 have a certain theoretical and applied interest. First, we note that, as in a Newtonian fluid, as U_∞ increases the transition point is shifted upstream. Second, moderate Na CMC concentrations (up to 1%) shift the x_{cr} in the direction of the trailing edge as a result of the simultaneous action of increased viscosity and the intensified pseudoplastic properties of the solution. The effect of the first factor is expressed through a decrease in Reynolds number; that of the second, as a more favorable ratio between the forces of inertia and friction drag. With further increase in polymer concentration this increase in x_{cr} ceases and an opposite tendency is distinctly observed—the transition region begins to move against the flow in the direction of the leading edge. An analysis of the experimental data yields the following empirical relation for the transition point, which is valid for our range of variation of the experimental parameters:

$$10^2 \leqslant \frac{\rho U_\infty^{2-n} x_{cr}^n}{k} \leqslant 5\cdot 10^4. \qquad (37)$$

In [9] the following rough estimate is given for the abscissa of the transition from a laminar to a turbulent layer:

$$3\cdot 10^5 < \left[\frac{0.332}{A(n)}\right]^2 \left(\frac{x_{cr}^n U_\infty^{2-n}\rho}{k}\right)^{\frac{2}{1+n}} < 3\cdot 10^6. \qquad (38)$$

The auxiliary quantity A(n), taken from the approximate calculations of Acrivos et al. [10], varies from 0.8 to 0.332 on the interval $0.1 \leq n \leq 1$. In Fig. 4 Skelland's approximation is compared with our data. The agreement is very satisfactory, and the deviation does not exceed ±4%. It is interesting to note that: a) the numerical value of the complex figuring in Skelland's inequality almost coincides with the value of the generalized Reynolds number; b) the left-hand limit of inequality (37) is much lower than in (38). Evidently, at considerable polymer contents the value of Re_{cr} depends not only on the shear viscosity characteristics but also on the viscoelastic properties of the system;

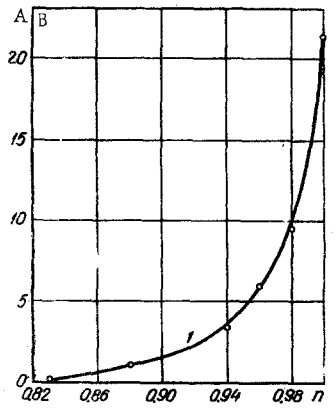

Fig. 4. Re_{cr} as a function of n (curve 1—Skelland approximation [9], points—our experimental data): A) from formula (37), B) from formula (38).

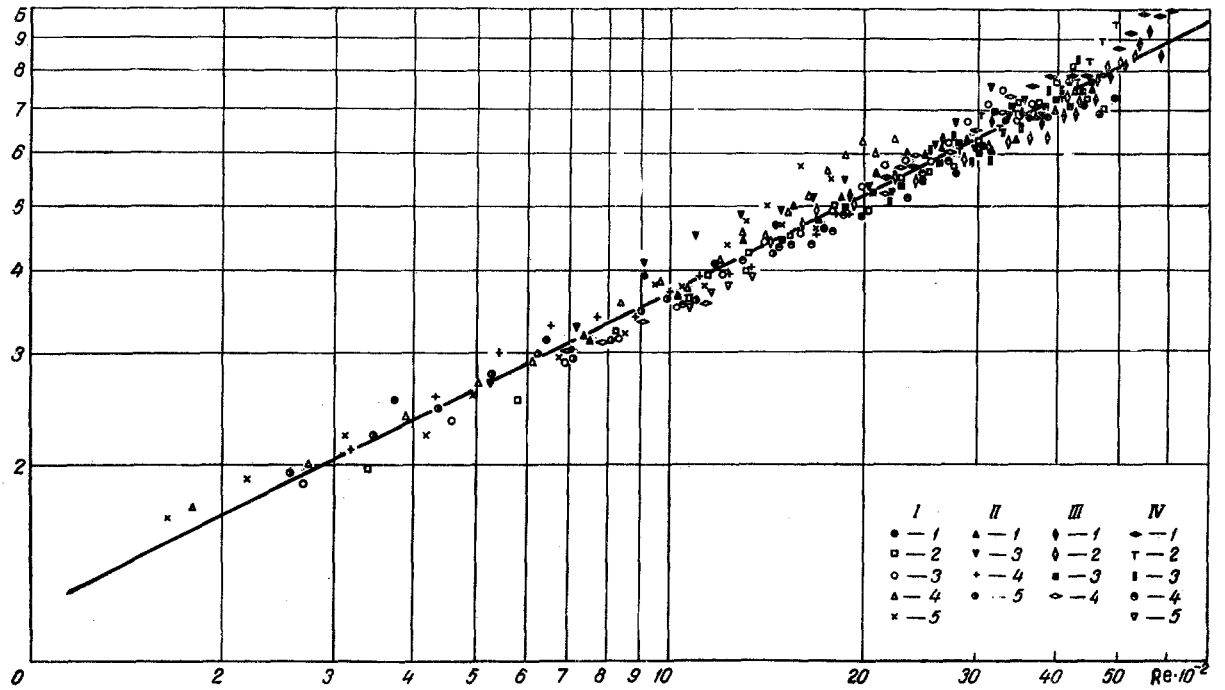

Fig. 5. Local mass fluxes at a plate in a longitudinal flow as a function of the Reynolds number at C_{CMC} = = 0%. Equation(30) (n = 1) is represented by the solid line: I)—n_0 = 0; II)—0.7 cm; III)—2.3; IV)—5.1; 1) u = = 50 cm/sec; 2) 45; 3) 35.2; 4) 21.2; 5) 17; $B = Nu_{mx}[1 - (h_0/x)^{3/4}]^{1/3} \cdot 10^{-2}$.

i. e., it is to a large extent determined by the size and configuration of the macromolecules and their concentration in the solution. This result and the conclusion that follows from it are also confirmed by the earlier data of Schnurmann [11, 12], who established for solutions of polyisobutylene and other macromolecules that $Re_{cr} \leq 10$.

The data, presented in Fig. 5, for the laminar part of the boundary layer of a Newtonian ECL solution are closely correlated with the known formula

$$Nu_m = A\,Re^{0.5}[1 - (h_0/x)^{3/4}]^{-1/3} \qquad (39)$$

(here, Pr_m has been fixed). Thus, the accuracy and reliability of the measurements based on the ECL method have again been demonstrated. The series of curves in Fig. 6 generalizes the results of the experiments with non-Newtonian ECL solutions. The analytic solution (30) is represented by the solid lines.

CONCLUSIONS

1) The experimental data for all Na CMC concentrations and various (h_0/x) are satisfactorily correlated when expressed in terms of the complexes $Nu_m Pe^{-1/3}\left[1 - \left(\frac{h_0}{x}\right)^{\frac{2n+1}{2(n+1)}}\right]^{-1/3}$ and Re. As distinct from the frequently used complex $Nu_m Pe^{-1/3}$, the product $Nu_m Pe^{-1/3}$ does not explicitly contain the rheological parameters n and k. The greater spread of the experimental points at low Na CMC concentrations and small Re is evidently associated with disturbances introduced into the boundary layer from the wake.

2) The analytic solution of the problem (30) suitably generalizes the experimental data at concentrations up to 1%. Consequently, the nonlinearity of the D(c) curve does not have much effect on the diffusion flow to the wall. The systematic deviation of the experimental points from the theoretical relation (30) for $c_0 = 1.5\%$ is attributable both to the nonlinearity of the diffusion coefficient and to the elasticoviscous behavior of the ECL solution. Kotaka [7] has established that for aqueous solutions of Na CMC of the alkaline type (with pH > 9) at flow shear rates of 10^3 sec^{-1}, the normal stress differences already appreciably exceed the shear stresses. It may also be assumed that the elasticoviscous properties begin to appear earlier, but that their influence on the j fluxes is compensated by the strong nonlinearity of the concentration dependence of the diffusion coefficient on the ascending branch of the D(c) curve. In the descending region of the D(c) curve ($c \approx 1\%$), the elasticoviscous properties should have a stronger influence on the local Nusselt number Nu_m.

NOTATION

k and n are the rheological parameters of the constitutive power equation; τ is the shear stress; $F(\eta)$ is a dimensionless stream function; $Re_{cr} = U_\infty x_{cr}/\nu_{eff}$ is the critical Reynolds number for a Newtonian fluid; $Pe_m = U_\infty x/D$ is the local (mass transfer) Peclet number; $Nu_m = jx/Dc_0$ is the local (mass transfer) Nusselt number; $Re = U_\infty^{2-n} x^n \rho/k$ is the generalized Reynolds number. Subscripts: m refers to mass transfer; lim represents limiting; 0 means remote from the wall, in the fluid volume; cr refers to critical.

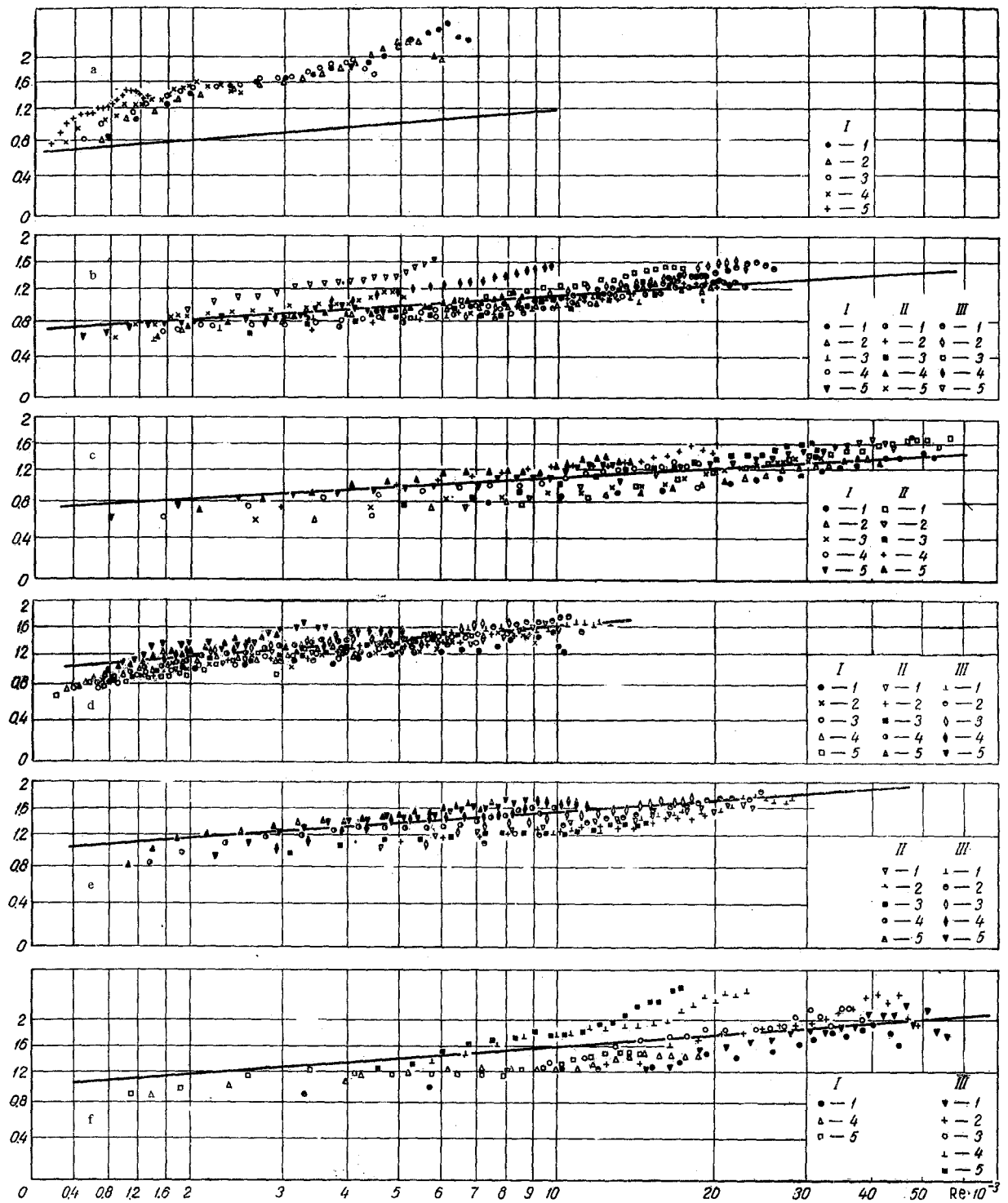

Fig. 6. Local mass fluxes at a plate in a longitudinal flow as a function of the Reynolds number. Equation (30) is represented by the solid line (a—C_{CMC} = 1.5%; b—1; c—0.75; d—0.5; e—0.25; f—0.1): I)—h_0 = 0; II)—0.7; III)—2.3; 1) u = 50 cm/sec; 2) 45; 3) 35.2; 4) 21.2; 5) 17; $B = Nu_{mx}Pe^{-1/3}\{1 - (h_0/x)\exp[(2n+1)/2(n+1)]\}^{1/3}$.

REFERENCES

1. Z. P. Shul'man and B. M. Berkovskii, Boundary Layer of Non-Newtonian Fluids [in Russian], Nauka i tekhnika, Minsk, 1966.

2. V. G. Levich, Physicochemical Hydrodynamics [in Russian], Fizmatgiz, 1959.

3. B. Howland, G. S. Springer, and M. G. Hill, Journal Fluid Mech., 24, part 4, 697, 1966.

4. G. S. Springer, Rev. Scient. Instr., 35, 1277, 1964.

5. A. V. Luikov, Z. P. Shul'man, and B. I. Puris, IFZh [Journal of Engineering Physics], 14, no. 1, 1968.

6. S. Goldstein, ed., Modern Developments in Fluid Dynamics [Russian translation], IL, Moscow, 1948.

7. T. Kotaka, M. Kurata, and M. Tamura, Journal Appl. Phys., 30, no. 11, 1959.

8. O. Lamm, Nova acta Regial Soc. Scient. Upsala, ser. 4, 10, no. 6, 1937.

9. A. H. P. Skelland, AIChE Journal, 12, 69, 1966.

10. Acrivos et al., AIChE Journal, 6, 312, 1960.

11. R. Schnurmann, Proc. First Intern. Rheol. Congr. Scheveningen, part 2, p. 142, 1949.

12. F. R. Eirich, ed., Rheology, Theory and Application [Russian translation], IL, Moscow, p. 701, 1962.

11 January 1968

Institute of Heat and Mass Transfer AS BSSR, Minsk